Computation of turbulent Prandtl number for mixed convection around a heated cylinder

By S. Kang AND G. Iaccarino

1. Motivation and objectives

Turbulent flow problems with conjugate heat transfer have been very important in engineering for a wide range of industrial applications. For example, accurate prediction of the interaction of the heat flux across the fluid-solid interface is very useful for designing thermal components.

In the literature, conjugate heat transfer in turbulent flows has been widely investigated. The majority of the studies have used RANS-based models (Yan 1995; Papanicolaou *et al.* 2001; Huang & Chun 2003; Hsieh & Lien 2005, among others). Only a few studies have used LES or DNS for conjugate heat transfer problems (Tiselj *et al.* 2001; Smirnova & Kalaev 2004; Kang *et al.* 2009*a*). Iaccarino & Moreau (2006) applied the immersed boundary (IB) method to conjugate heat transfer problems using a RANS model. Yu *et al.* (2006) applied a distributed Lagrange multiplier-based fictitious domain method to a conjugate heat transfer problem of a particulate flow at low Reynolds number. Recently, Kang *et al.* (2009*a*) used the IB method as an efficient tool to perform a DNS study of a turbulent conjugate heat transfer problem. The IB method is a numerical technique to enforce boundary conditions on surfaces not aligned with the mesh. As noted in Kang *et al.*, an advantage of the IB method is its capability of handling multi-phase or multi-material problems. More specifically, the interface between different materials can be regarded as an immersed boundary. The IB method is then equivalent to the imposition of physical conditions at the interface.

There are two objectives of the present study. The first is to apply a revised IB method to a turbulent conjugate heat transfer problem. A heated cylinder in a channel with heating from below considered in Laskowski *et al.* (2007) is a very interesting problem because it includes many complex and interesting flow phenomena such as transition and turbulent natural convection. The revised method is supposed to reduce the error compared to the existing method by Kang *et al.*. The second objective is computation and analysis of the turbulent Prandtl number (Pr_t). This number has been very important as a RANS modeling parameter as well as for its physical meaning. Typically, Pr_t is assumed to be unity for several reasons (i.e., the Reynolds analogy). Although this assumption is valid for important building block problems such as the boundary layer and pipe, there has been some doubt about its validity for more complex applications. When a problem has several flow features (e.g., a flow in a complex geometry or in a transitional regime), the assumption of a single value for Pr_t in the entire domain may be invalid. In the present study, the validity of the Reynolds analogy is evaluated for the problem with various flow features considered in Laskowski *et al.*

In the next section, numerical methods including a revised IB method for conjugate heat transfer will be described. The proposed method is validated against an analytic solution. In the third section, statistical results from DNS of a heated cylinder in a channel with heating from below will be presented, followed by the conclusion.

2. Numerical methods

2.1. *Description of the Navier-Stokes solvers*

In the present study, a heat transfer problem with mixed convection is considered. The variable density formulation of the Navier-Stokes equations is written as

$$\frac{\partial \rho u_i}{\partial t} + \frac{\partial \rho u_i u_j}{\partial x_j} = -\frac{\partial p}{\partial x_i} + \frac{\partial}{\partial x_j}\left[\mu\left(\frac{\partial u_i}{\partial x_j} + \frac{\partial u_j}{\partial x_i}\right)\right] + \rho g_i, \tag{2.1}$$

$$\frac{\partial \rho}{\partial t} + \frac{\partial \rho u_i}{\partial x_i} = 0, \tag{2.2}$$

$$\frac{\partial \rho h}{\partial t} + \frac{\partial \rho u_j h}{\partial x_j} = \frac{\partial}{\partial x_j}\left[k\frac{\partial T}{\partial x_j}\right], \tag{2.3}$$

where t is the time, ρ is the density, u_i is the velocity, p is the pressure, μ is the molecular viscosity and g_i is the vector of the gravitational acceleration. T is the temperature, $h = c_p T$ is the enthalpy and k is the thermal conductivity.

The solution to the Navier-Stokes equations Eqs. (2.1)−(2.3) is obtained using a fully implicit LES solver based on a finite volume method (FVM) called CDP†. In order to achieve optimal control of the grid size, locally refined meshes (i.e., a mesh consisting of hexahedral elements with hanging nodes) are used with the IB method. In the present study, elements around hanging nodes are treated as unstructured polyhedral control volumes. Further details on local mesh refinement in the present study are available in Kang *et al.* (2009*b*).

2.2. *Immersed boundary method for a multi-material problem (conjugate heat transfer)*

The present study uses the IB method as an efficient tool to handle conjugate heat transfer problems. This approach is a revised version of the method of Kang *et al.* (2009*a*). In this section, the approach of Kang *et al.* is briefly introduced, and then a revised version using a Hermite-type interpolation is described.

Figure 1 shows the two steps necessary to build communication across the interface between two adjoining materials. Starting from the true fluid-solid interface, two approximated boundaries (Γ_{fluid} and Γ_{solid}) facing each other across the true interface are constructed. The next stage is to build connections between points on the two approximated boundaries. If grid points on the approximated boundaries are projected onto the true material interface as shown in Figure 1(b), a linear interpolation is possible between the groups of gray and black points in order to communicate information across the interface.

The data communicated across the material interface are specific to the conjugate heat transfer problem:

$$T_{fluid} = \overline{T_{solid}} \tag{2.4}$$

$$k_{solid}\left.\frac{\partial T}{\partial \boldsymbol{n}}\right|_{solid} = \overline{k_{fluid}\left.\frac{\partial T}{\partial \boldsymbol{n}}\right|_{fluid}}, \tag{2.5}$$

where $\mathbf{n}$ denotes the normal to the true interface, k denotes the thermal conductivity of a material, and the overbar denotes an interpolated value. These conditions are adapted as asymmetric boundary conditions. The wall-normal heat flux is computed from the reconstruction formula for imposing the boundary conditions, which is equivalent to a

† CDP is named for Charles David Pierce (1969−2002)

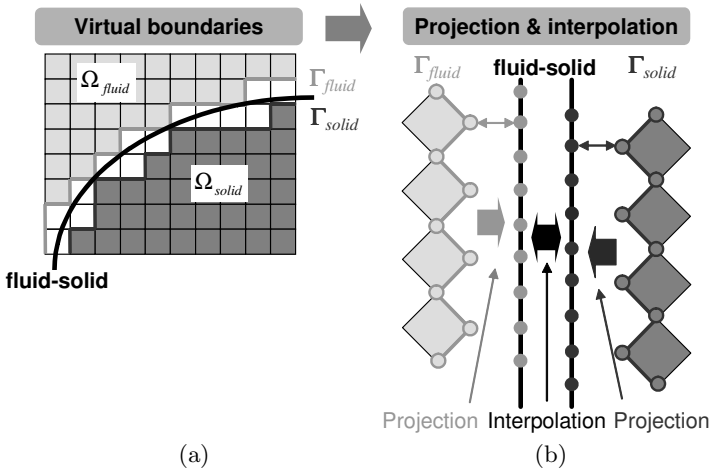

FIGURE 1. Schematic diagrams for interface treatment between different materials: (a) construction of approximated boundaries facing each other (Γ_{fluid} and Γ_{solid}) across the fluid-solid interface; (b) computation of interpolation coefficients from the projected boundaries.

one-sided finite difference. In the matrix solution step, Eqs. (2.4)−(2.5) are satisfied in an iterative procedure. Once the interpolated B.C. is updated, the B.C. is enforced at the IB using the reconstruction method of Kang *et al.* (2009*a*) with a linear interpolation method.

A limitation of this approach is a low-order accuracy from the one-sided finite difference with first-order accuracy. In the present study, we aim to relax this limitation by employing a Hermite-type interpolation method. The Hermite interpolation achieves a high-order accuracy with a compact stencil by using the gradient as well as the value at each grid point. By adapting this approach to the present configuration (Figure 1), a quadratic interpolation can be achieved by using both the temperature value and its gradient. The computational overhead is minimal because the width of the original stencil that requires information within one grid point away is maintained.

The proposed approach can be understood as adding correction terms to the original conditions with the linear reconstruction. Then, Eqs. (2.4)−(2.5) can be written as

$$T_{fluid} = \overline{T|_{solid}^{linear}} + \overline{\Delta T|_{solid}^{quad}} \tag{2.6}$$

$$k_{solid}\left.\frac{\partial T}{\partial \boldsymbol{n}}\right|_{solid} = \overline{k_{fluid}\left(\left.\frac{\partial T}{\partial \boldsymbol{n}}\right|_{fluid}^{linear} + \Delta\left.\frac{\partial T}{\partial \boldsymbol{n}}\right|_{fluid}^{quad}\right)}, \tag{2.7}$$

where Δ denotes the correction from the quadratic interpolation. The present approach is nominally second-order. A requirement is that the gradient should be computed in an accurate way. In the next section, this approach will be compared with the original method of Kang *et al.* (2009*a*).

2.3. *Verification study*

The accuracy of the method in Section 2.2 was verified with a two-dimensional laminar test case.

Figure 2(a) shows a schematic diagram of a heat transfer problem between two coannular cylinders. A fluid is rotating between the inner and outer cylinders. The outer

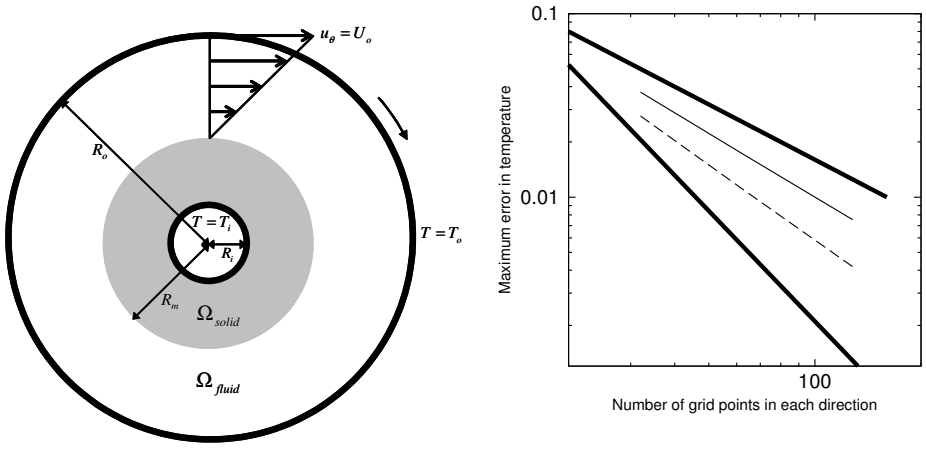

(a) (b)

FIGURE 2. A conjugate heat transfer problem of a rotating flow between two coannular cylinders: (a) schematic diagram; (b) maximum errors in the temperature: ——— , the result of Kang *et al.* (2009*a*); - - - - , the present study with Hermite interpolation. The thick solid lines show first and second order accuracy.

cylinder is rotating so that the radial velocity at the wall is U_o, while the inner cylinder is stationary. The temperature is set to a fixed value at the inner wall of the inner cylinder and at the wall of the outer cylinder. The energy balance Eqs. (2.4)−(2.5) are satisfied at the interface between the fluid and inner cylinder. The radius of the inner and outer walls of the inner cylinder and the wall of the outer cylinder is R_i=0.45, R_m=0.9 and R_o=1.8, respectively. The ratio of constant heat conductivities between the solid and fluid is set to 9. The analytic solution to this problem is

$$u_\theta = 0,\ u_r(r) = \begin{cases} 0 & \text{for } R_i < r < R_m \text{ (solid)} \\ -\frac{R_o R_m^2 U_o}{R_o^2 - R_m^2}\frac{1}{r} + \frac{R_o U_o}{R_o^2 - R_m^2} r & \text{for } R_m < r < R_o \text{ (fluid)} \end{cases} \tag{2.8}$$

$$T(r) = \begin{cases} T_i + \frac{T_o - T_i}{\log(R_m/R_i) + (k_s/k_f)\log(R_o/R_m)} \log(\frac{r}{R_i}) & \text{for } R_i < r < R_m \\ T_o - \frac{T_o - T_i}{(k_f/k_s)\log(R_m/R_i) + \log(R_o/R_m)} \log(\frac{R_o}{r}) & \text{for } R_m < r < R_o \end{cases}, \tag{2.9}$$

where r and θ denote the radial and azimuthal directions. Steady velocity and temperature fields were computed for three different grid spacings. The accuracy was then deduced by comparing the maximum error versus the grid spacing.

Figure 2(b) shows the maximum error in the temperature. Specifically, the method proposed in the previous section is compared with the method used in Kang *et al.* (2009*a*). The temperature shows an accuracy less than second-order, but higher than the first-order observed in Kang *et al.* Compared to the previous linear interpolation method, the accuracy becomes a little higher and the size of the error is reduced by approximately 40% with the Hermite interpolation method. Although this result shows the effectiveness of the proposed method, the accuracy is still lower than second-order. The reason is that the gradient value in the Hermite interpolation is based on the one-sided finite-difference and is supposed to have a lower accuracy than a symmetric finite-difference. This error affects the overall accuracy of the Hermite interpolation.

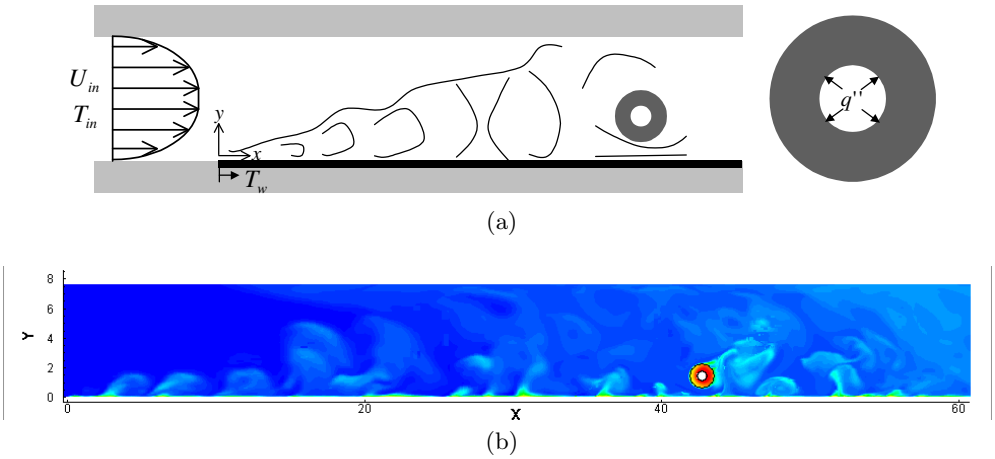

FIGURE 3. A heated cylinder inside a channel heated from below: (a) schematic diagram; (b) contours of the instantaneous temperature field.

3. A heated cylinder in a channel heated from below

3.1. *Case description and computational setup*

Figure 3 shows the configuration used in Laskowski *et al.* (2007) and Kang *et al.* (2009*a*) and the contours of the instantaneous temperature field. The bottom wall is heated to a high temperature from the streamwise (x) location $x = 0$. This surface heating results in a thermal boundary layer developing along the bottom wall. A horizontal tube made of stainless steel is placed along the spanwise (z) direction. The outer and inner walls of the tube are referred to as the outer and the inner cylinder, respectively. Inside the inner cylinder, a flow of hot water heats the tube. The Reynolds number, based on the mean streamwise velocity (U_{in}) and the channel half-width ($H/2$), is approximately 414. This Reynolds number corresponds to a laminar flow, but thermal plumes generated by the buoyancy force trigger transition to turbulence.

The size of the domain is the same as in Kang *et al.* (2009*a*), i.e., the length (L) and height (H) of the test section in the experiment are 61 cm and 7.62 cm, respectively. The spanwise domain size is reduced from 61 cm to 15 cm to limit the computational cost. The size of the smallest coherent structure is observed to be less than 1.3 cm in the spanwise direction. The streamwise and wall-normal location of the center of the tube is (42.7 cm, 1.43 cm). The diameters of the inner and outer cylinders are 6.35 mm and 15.875 mm, respectively. With regard to the inlet velocity, an interpolated velocity profile from the experiment is used. This velocity B.C. is steady in time, even though unsteady effects might be present in the experiment. The velocity B.C. at the walls is the no-slip condition. The inlet temperature is used as the Dirichlet B.C. at the inlet. The temperature at the bottom wall is 318 K, while the top wall is adiabatic. The temporally and spatially averaged temperature at the outer cylinder is 311.3 K. Since the heat flux at the inner cylinder was not measured, we assume it was constant. The value of the constant heat flux is adjusted during the simulation such that the measured averaged temperature at the outer cylinder matches the value from the experiment. Material properties such as the viscosity, density, thermal conductivity and specific heat at constant pressure are tabulated as functions of the temperature and updated during the simulation for each grid point.

In regard to the mesh, Kang *et al.* (2009*a*) performed a grid study to find a reasonable

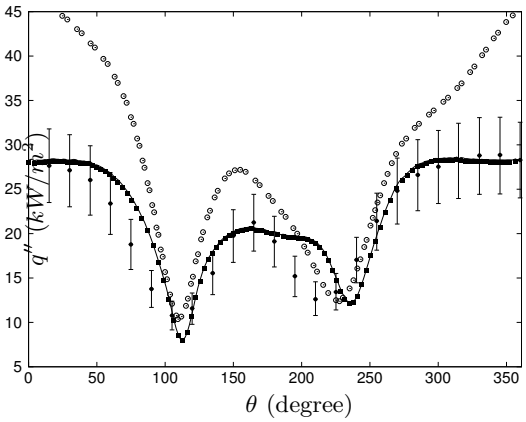

FIGURE 4. The time-averaged heat flux at the outer cylinder: •, experiment (Laskowski *et al.* 2007); ⊙, RANS (Laskowski *et al.* 2007); ■, Kang *et al.* (2009*a*); ——— , the present study with Hermite interpolation. $\theta = 0^\circ$ and 90° correspond to the forward stagnation point and the top of the cylinder.

resolution. In the present study, the finest mesh tested in Kang *et al.* is used. The total number of mesh points is approximately 12 million. Statistics is averaged in both time and spanwise direction. The computational time step used for averaging is about 40,000.

3.2. *Results*

In order to validate the revised IB method for the conjugate heat transfer problem, the averaged heat flux at the outer cylinder is compared with the result of Kang *et al.* (2009*a*).

Figure 4 shows the averaged heat flux computed in the present study. Almost the same result as that of Kang *et al.* (2009*a*) is observed, which implies that the effect of the smaller error from the fluid-solid interface is minimal to the averaged heat flux. Discrepancies between the DNS and the experiment are observed near the local maxima of the heat flux.

Figure 5 shows a correlation between the velocity and temperature fluctuations $\langle T'v' \rangle$ and $\langle u'v' \rangle$. In Figure 5(a), we can identify the coherent structures of thermal plumes developing from the bottom wall with the large values of $\langle T'v' \rangle$. Interestingly, the organized structures are observed even after the flow becomes turbulent (e.g., downstream of the cylinder). Notably, the coherent thermal plumes are not clearly observed from $\langle u'v' \rangle$ in Figure 5(b) except for the region close to the inlet. This result implies that, once turbulent flow structures are produced, the Reynolds stress $\langle u'v' \rangle$ is not strongly affected by the thermal plumes.

One of the objectives of the present study is to compute the turbulent Prandtl number (Pr_t). In its conventional definition (e.g., for a boundary layer), the Pr_t is written as

$$Pr_t = \frac{\nu_t}{\alpha_t} = \frac{\langle u'v' \rangle \frac{\partial \langle T \rangle}{\partial y}}{\langle T'v' \rangle \frac{\partial \langle U \rangle}{\partial y}}. \tag{3.1}$$

Figure 6 shows the turbulent Prandtl number near the bottom wall. From the inlet to the cylinder location (x=42 cm), the flow is understood as a transitional thermal boundary layer. We can see different trends across $x \approx 7$ cm. Before $x \approx 7$ cm, occasional large values corresponding to initial thermal plumes are observed in the background of

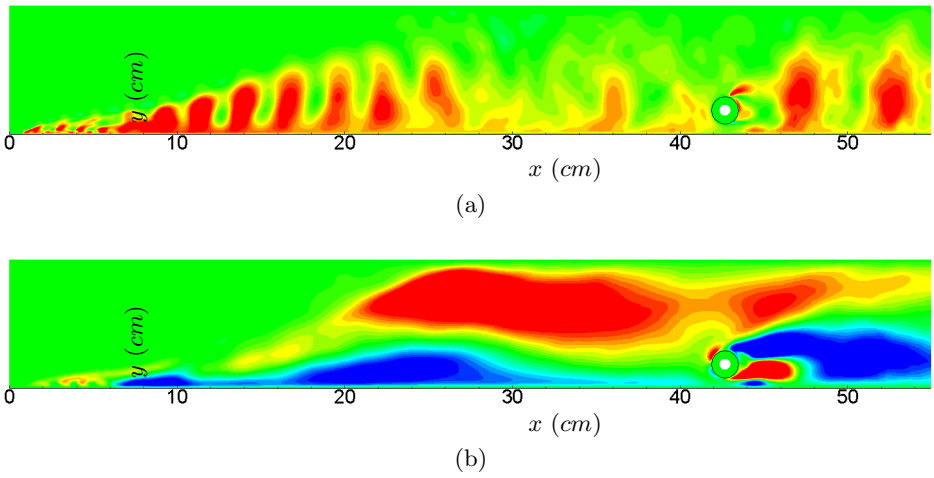

FIGURE 5. Contours of correlation of the temperature and velocity fluctuation components: (a) $\langle T'v' \rangle$; (b) $\langle u'v' \rangle$. Twenty contour levels are used in the range of -1 to 1 for $\langle T'v' \rangle$ and -0.07 to 0.07 for $\langle u'v' \rangle$.

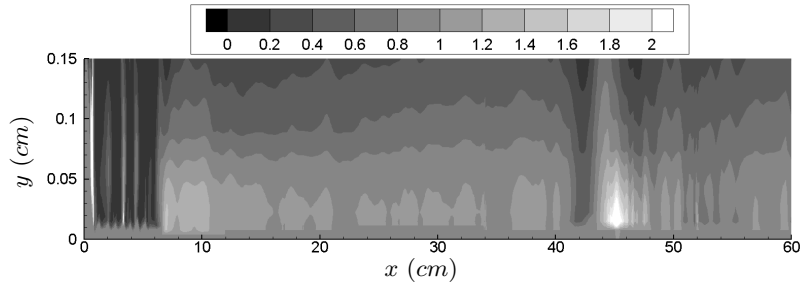

FIGURE 6. Contours of the turbulent Prandtl number defined in Eq. (3.1) near the bottom wall.

very small value corresponding to the laminar boundary layer. After $x \approx 7$ cm, the Pr_t shows the typical trend of a turbulent boundary layer – has the value between 1∼1.3 nearby y=0.01∼0.05 cm and decreases as y increases. These results agree quantitatively well with the previous studies such as those of Blackwell (1973) and Kays & Crawford (1993) for turbulent boundary layers.

In the present study, the flow in a channel interacts with a circular cylinder. Thus, we considered another definition of the turbulent Prandtl number valid nearby the circular cylinder:

$$Pr_t = \frac{\nu_t}{\alpha_t} = \frac{\langle u_t' u_n' \rangle \frac{\partial \langle T \rangle}{\partial n}}{\langle T' u_n' \rangle \frac{\partial \langle U_t \rangle}{\partial n}}, \tag{3.2}$$

where n and t denote the normal and tangential coordinate to the local cylinder surface, respectively.

Figure 7 shows the contours of turbulent Prandtl number defined in Eq. (3.2) near the cylinder. Although some of the contours are rough because of insufficient samples, it is observed that the Pr_t has a relatively large value near the front ($\theta \approx 350°$) and the entire rear part ($\theta = 100 \sim 180°$) of the cylinder. The Pr_t value rapidly changes in space and

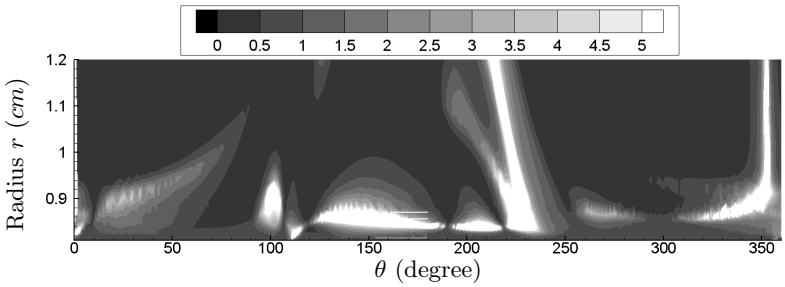

FIGURE 7. Contours of the turbulent Prandtl number defined in Eq. (3.2) near the outer cylinder wall. θ=0° and 90° correspond to the forward stagnation point and the top of the cylinder and the radius r =0.795 cm corresponds to the outer cylinder wall.

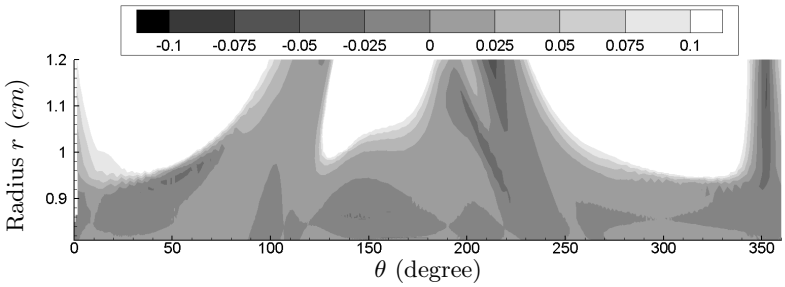

FIGURE 8. Contours of the difference between turbulent diffusivity and viscosity (= $\alpha_t - \nu_t$) computed from the DNS result using Eqs. (3.3) and (3.4). $\theta = 0°$ and 90° correspond to the forward stagnation point and the top of the cylinder, and the radius r =0.795 cm corresponds to the outer cylinder wall.

shows a wide range from 0.1 to 20. This wide range of Pr_t can raise an issue in RANS modeling where a fixed value is usually assumed.

In order to deduce the effect of the constant Pr_t assumption such as the Reynolds analogy (Pr_t=1) on turbulence modeling, we compared the turbulent diffusivity α_t evaluated from our DNS result with the α_t from the Reynolds analogy ($\alpha_t = \nu_t$). The turbulent diffusivity and viscosity valid nearby the cylinder is written as

$$\alpha_t = -\langle T' u_n' \rangle / \frac{\partial \langle T \rangle}{\partial n}, \tag{3.3}$$

$$\nu_t = -\langle u_t' u_n' \rangle / \frac{\partial \langle U_t \rangle}{\partial n}. \tag{3.4}$$

Figure 8 shows the difference between the α_t evaluated from our DNS and the Reynolds analogy (= $\alpha_t - \nu_t$). The difference is small close to the cylinder (small r) but becomes large as the distance increases from the wall. Notably, the difference is relatively small near $\theta = 110°$ and 220° even when the radius r is relatively large. Interestingly, these regions correspond to the regions where the averaged heat flux from the RANS (Laskowski *et al.* 2007) agrees well with the experiment as shown in Figure 4. Considering that an assumption on the Pr_t such as the Reynolds analogy must be used in Laskowski *et al.* (2007), the fixed Pr_t value in the RANS simulation may be a reason for the large difference of the averaged heat flux from the experiment. In the regions with a large difference of ($\alpha_t - \nu_t$) in Figure 8, the Pr_t value should be greater than 1. If we can include the effect of the large Pr_t in the RANS simulation, the increased total diffusivity

($\alpha_{mol} + \alpha_t$) can result in a thicker thermal boundary layer which leads to a smaller heat flux. From Figure 4, we can see that this change results in a better agreement of the RANS result with the experiment. Thus, the approach to include the effect of the variable Pr_t in a RANS simulation seems to be attractive, but a universal definition of Pr_t that works in the entire domain is necessary.

4. Conclusions

The objectives of the present study are to propose a revised reconstruction method for conjugate heat transfer and analysis of the turbulent Prandtl number for a turbulent flow in a complex geometry. The revised method for conjugate heat transfer is based on the IB method which has become popular for flow problems involving very complex geometries and moving bodies. We revised the existing method of Kang *et al.* (2009*a*) with a Hermite-type interpolation which can improve the accuracy without increasing the width of the computational stencil. When applied to a verification problem with an analytic solution, the revised method decreases the error by approximately 40%.

When the proposed method is applied to a problem of a heated cylinder in a channel with heating from below, the agreement of the time-averaged heat flux at the cylinder outer wall with the experiment is satisfactory. The turbulent Prandtl number near the bottom wall shows quantitatively reasonable agreement with the previous studies. The turbulent Prandtl number nearby the cylinder shows a large variation in space, which implies that the assumption of a single value in the entire flow domain is invalid for the present application. Further analysis suggests that inclusion of the effect of the variable Pr_t results in a better agreement of the RANS result with the previous experiment.

Acknowledgments

Financial support from the Center for Turbulence Research (CTR) and NASA is gratefully acknowledged. We also thank the authors of Laskowski *et al.* (2007) for their experimental data and suggestions.

REFERENCES

Blackwell, B. F. 1973 The turbulent boundary layer on a porous plate: an experimental study of the heat transfer behavior with adverse pressure gradients. PhD thesis, Stanford University.

Hsieh, K. J. & Lien, F. S. 2005 Conjugate turbulent forced convection in a channel with an array of ribs. *Int. J. Numer. Meth. Heat Fluid Flow* **15** (5), 462–482.

Huang, S. & Chun, C.-H. 2003 A numerical study of turbulent flow and conjugate heat transfer in concentric annuli with moving inner rod. *Int. J. Heat Mass Transfer* **46**, 3707–3716.

Iaccarino, G. & Moreau, S. 2006 Natural and forced conjugate heat transfer in complex geometries on Cartesian adapted grids. *J. Fluids Engng.* **128**, 838–846.

Kang, S., Iaccarino, G. & Ham, F. 2009*a* DNS of buoyancy-dominated turbulent flows on a bluff body using the immersed boundary method. *J. Comput. Phys.* **228**, 3189–3208.

Kang, S., Iaccarino, G., Ham, F. & Moin, P. 2009*b* Prediction of wall-pressure

fluctuation in turbulent flows with an immersed boundary method. *J. Comput. Phys.* **228**, 6753–6772.

Kays, W. M. & Crawford, M. E. 1993 *Convective Heat and Mass Transfer*, 3rd edn. McGraw-Hill.

Laskowski, G. M., Kearney, S. P., Evans, G. & Greif, R. 2007 Mixed convection heat transfer to and from a horizontal cylinder in cross-flow with heating from below. *Int. J. Heat Fluid Flow* **28**, 454–468.

Papanicolaou, E., Giebert, D., Koch, R. & Schulz, A. 2001 A conservation-based discretization approach for conjugate heat transfer calculations in hot-gas ducting turbomachinery components. *Int. J. Heat Mass Transfer* **44**, 3413–3429.

Smirnova, O. V. & Kalaev, V. V. 2004 3D unsteady numerical analysis of conjugate heat transport and turbulent/laminar flows in LEC growth of GaAs crystals. *Int. J. Heat Mass Transfer* **47**, 363–371.

Tiselj, I., Bergant, R., Mavko, B., Bajsic, I. & Hetsroni, G. 2001 DNS of turbulent heat transfer in channel flow with heat conduction in the solid wall. *J. Heat Transfer-Trans. ASME* **123**, 849–857.

Yan, W.-M. 1995 Unsteady conjugated heat transfer in turbulent channel flows with convection from the ambient. *Int. J. Heat Mass Transfer* **38**, 2101–2108.

Yu, Z. S., Shao, X. M. & Wachs, A. 2006 A fictitious domain method for particulate flows with heat transfer. *J. Comput. Phys.* **217** (2), 424–452.